A comprehensive study of dense zirconia components fabricated by additive manufacturing

Sun, Jinxing; Chen, Xiaoteng; Wade-Zhu, James; Binner, Jon; Bai, Jiaming

[Link to publication on Research at Birmingham portal](#)

A comprehensive study of dense zirconia components fabricated by additive manufacturing

Jinxing Sun[a,b], Xiaoteng Chen[a], Jon Binner[b], Jiaming Bai[a*]

a. Shenzhen Key Laboratory for Additive Manufacturing of High-performance Materials，Department of Mechanical and Energy Engineering, Southern University of Science and Technology, Shenzhen, 518055, China

b. School of Metallurgy and Materials, University of Birmingham, B15 2TT, UK

* Corresponding Author: baijm@sustech.edu.cn (J. Bai)

Abstract

Although additive manufacturing provides numerous potential advantages for fabricating functional, complex geometry zirconia parts with efficiency, industrial interest in practical applications is currently lacking. Hence, a comprehensive investigation into the performance offered by additively manufactured zirconia components will be beneficial for promoting industrial applications. The aim of this study is thus to provide a detailed evaluation of zirconia specimens fabricated by one of the most utilised ceramic additive manufacturing technologies, viz. digital light processing (DLP), with a range of typical zirconia components being printed. Key performance factors include the subsequent

densification and the resulting surface quality, dimensional accuracy, shrinkage, and mechanical properties. The results showed that the performance of the DLP-prepared zirconia parts was comparable to those of conventionally fabricated zirconia. It is believed that this paper will serve as a good reference for engineers and the industrial community.

1. Introduction

Additive manufacturing (AM) offers a near net shape route for the fabrication of advanced ceramics with highly complex geometries. It does not require the initial construction of a mould and hence is a fast-response technique to develop new products for designers and engineers [1,2,3]. To date, a number of different ceramic AM processes are being investigated, these can be listed in the following sequence in terms of frequency of use: vat-polymerisation based methods [4,5,6,7,8]; direct ink writing (also known as robocasting) [9,10,11,12]; binder jetting (BJ) [13,14,15,16]; inkjet printing (IJP) [17,18]; selective laser sintering / melting (SLS/SLM) [19,20,21]; laser engineered net shaping (LENS) [22,23] and emerging hybrid AM processes [24]. Each AM technology offers potential capabilities along with limitations. Whilst vat-polymerisation based techniques, such as digital light processing (DLP), are

gaining increasing interest for manufacturing ceramic parts due to high printing resolution, good surface finish and being a generically fast building process, they are, nevertheless, still in a relative stage of infancy compared with conventional ceramic processing.

As one of the most important ceramic materials, zirconia exhibits a particularly high flexural strength and toughness [25,26,27], as shown in Fig. 1, and also offers other advantages such as biocompatibility [28], high chemical and temperature resistance [29]. The resulting wide range of applications, many of which require complex-shaped parts, make zirconia a popular candidate for additive manufacturing and, in particular, DLP technology. As just one example, Marsico et al. [30] focused on an investigation into the mechanical properties of zirconia printed via DLP in five different build orientations in order to study and classify the influence of build orientation on the resulting Vicker's hardness, indentation fracture toughness and three point bend flexural strength. The conclusion reached was that although for some orientations the measured strengths were found to be comparable to the reference material considered, fracture was observed to initiate frequently at layer lines and related defects. The authors concluded that if the layer lines could be prevented or engineered, the strength of vat-printed ceramics could be substantially improved.
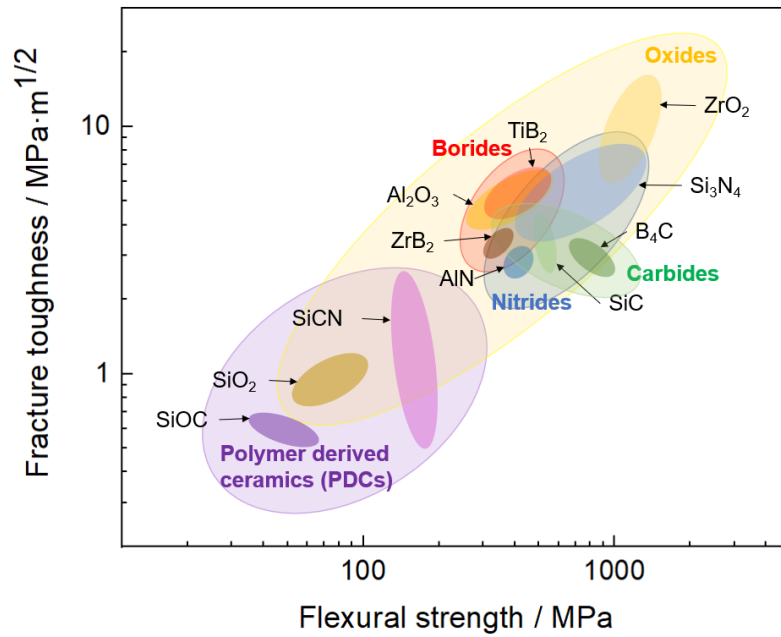
Fig. 1. Ashby plots for advanced ceramics. All data obtained from the studies [31,32,33,34,35,36].

This work provides a comprehensive study of DLP printed zirconia, with the specific aim of promoting its industrial application. The densification of printed zirconia was initially characterised by both simple density measurement and subsequent X-ray micro-computed tomography (microCT). In addition, the printing quality, dimensional accuracy, sintering shrinkage, surface roughness and microstructure of the sintered parts were analysed in detail. Furthermore, the mechanical properties, including Vickers hardness, fracture toughness and flexural strength were also characterised using relevant standards. Finally, to illustrate the potential of using DLP in the manufacturing of functional zirconia components, a range of representative structures were printed and sintered.

2. Experimental section

2.1 Sample preparation

Initially, zirconia green bodies were printed using highly zirconia loaded slurry on a DLP 3D printer with an UV light of 405 nm wavelength. A schematic of the DLP printing principles is shown in Fig. 2. The layer thickness was set as 25 μm for all the builds. A range of zirconia green bars, disks and components were obtained for subsequent characterisation and evaluation. Then, the fabricated green bodies were cleaned in an ultrasonic bath to remove the excess slurry. Finally, according to the results of thermogravimetric analysis, TGA (STA 449 *F5 Jupiter,* NETZSCH GmbH, Selb, Germany), shown in Fig. 3a, the debinding and sintering processes were conducted in a tubular furnace (GSL-1700X, Hefei Kejing Co. Ltd., Anhui, China) under an air flow following the profile shown in Fig. 3b. The final parts were subsequently obtained for evaluation.
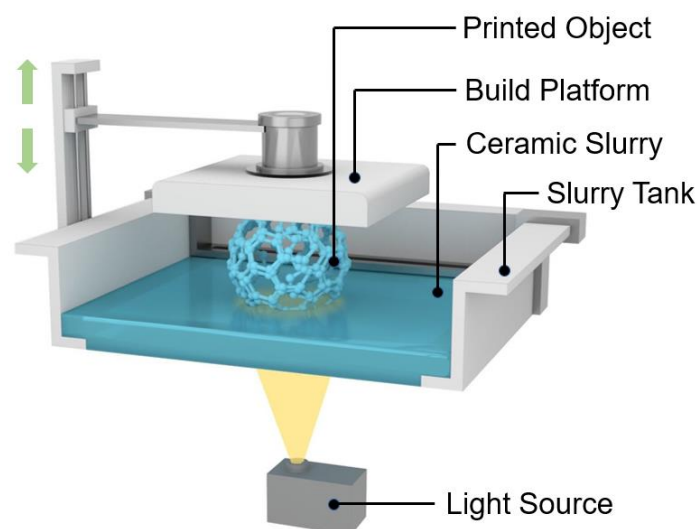
Fig. 2. Schematic of the printing principles of DLP.
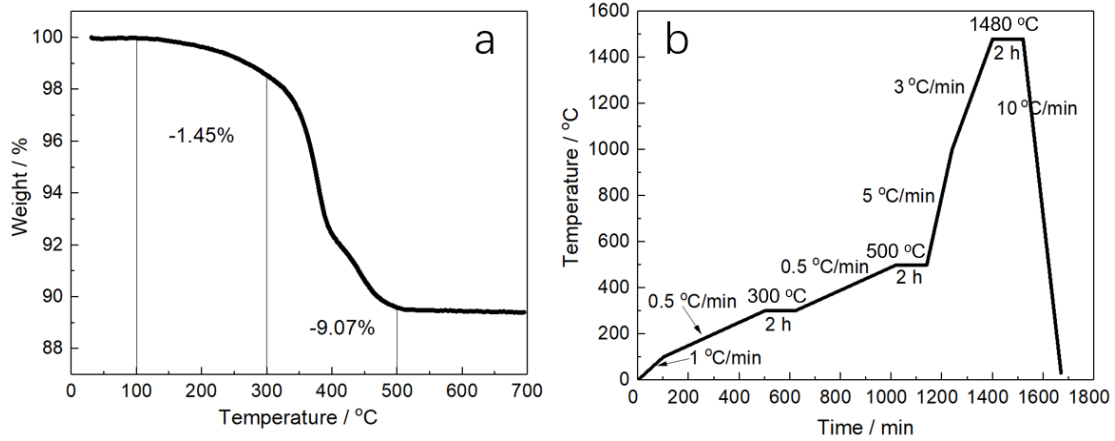
Fig. 3. (a): TGA result and (b) the debinding and sintering profile.

2.2 Characterisation

2.2.1 Densification analysis

The relative density of the sintered disks was determined according to the Archimedes principle with ethanol as the immersion fluid, where 30 zirconia disks with diameter of 5 mm and height of 3 mm were adopted. A micro-computed tomography (micro-CT) scanner (model d2, Diondo, Hattingen, Germany) was used to detect both internal and external defects in the DLP manufactured zirconia parts at 110 kV, where the 3D structure was subsequently recreated using VGStudio MAX 2.26 (Volume Graphics GmbH, Heidelberg, Germany).

2.2.2 Sintering shrinkage, dimensional accuracy and surface roughness

Sintered ceramic parts manufactured by DLP can suffer from shrinkage issues. A constructive method for resolving these is to compensate for this shrinkage

by applying an appropriate scaling factor in each direction to the CAD/CAM model before printing. Fig. 4 shows the dimensional changes from the 3D model to the final sintered parts with and without the shrinkage scaling factor being used, where the dimensions in three directions in the green body and final part stages were measured using a calliper (500-702-20, Mitutoyo, Kawasaki, Japan). In both cases, the linear shrinkage was assessed using 20 test bars with designed dimensions of 45 x 4 x 3 mm, with the shrinkage scaling factor being applied to one set of 20 test bars. Additionally, the surface roughness of the top, bottom and all the side surfaces were investigated quantitatively in the as-sintered condition by the arithmetic mean value of the profile (Ra) using a laser scanning confocal microscopy (LSCM, Keyence VK-X1000, Japan).

NB: L_1 = L x scaling factor W_1 = W x scaling factor H_1 = H x scaling factor
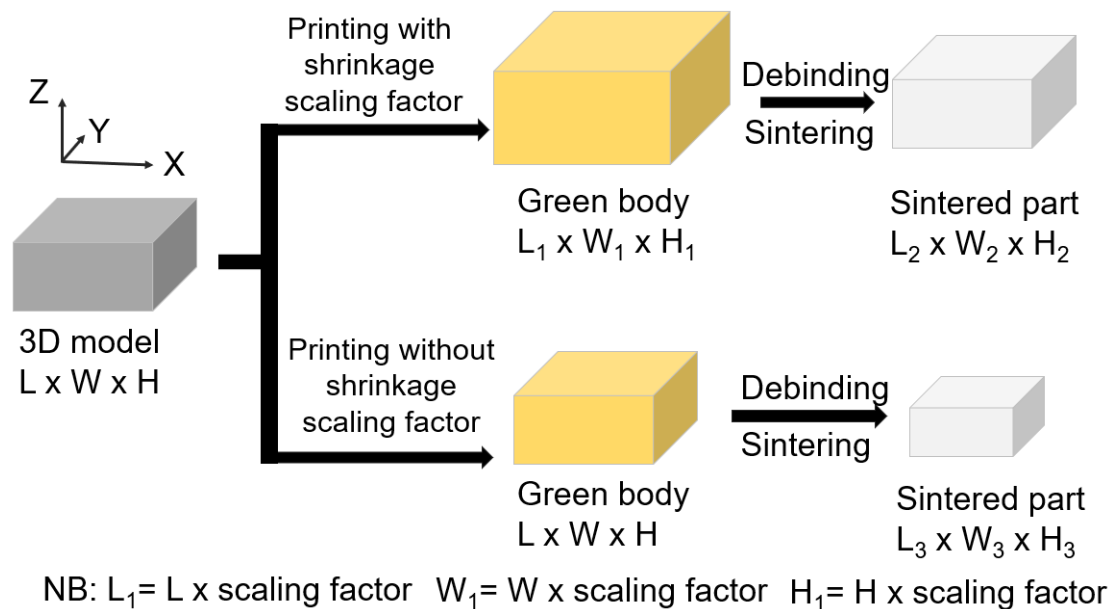
Fig. 4. Schematic diagram of the dimensional change in the process of zirconia DLP route.

Table 1. Formulas for linear shrinkage and dimensional accuracy.

	X direction (L)	Y direction (W)	Z direction (H)
Linear shrinkage	$\dfrac{L - L_3}{L} * 100\%$	$\dfrac{W - W_3}{W} * 100\%$	$\dfrac{H - H_3}{H} * 100\%$
Dimensional accuracy	$\dfrac{L_2 - L}{L} * 100\%$	$\dfrac{W_2 - W}{W} * 100\%$	$\dfrac{H_2 - H}{H} * 100\%$

2.2.3 Microstructure study

The microstructure of the parts and fracture surfaces were observed using scanning electron microscopy (FESEM, ZEISS Merlin, Oberkochen Germany). To obtain the desired grain size, the SEM samples were polished and then thermally etched at 1400°C to reveal the grain boundary network, followed by coating with a layer of Pt using a sputter coater. The average grain size was measured using the SEM image containing more than 400 individual grains by the lineal intercept technique [37].

2.2.4 XRD analysis

The phase transformation (t-m) analysis before and after fracture was performed by X-ray diffractometry XRD (Smartlab, Rigaku, Tokyo, Japan) using 2θ ranging between 20° and 80°, where the diffractometer was used with Cu Kα radiation at 40 mA and 45 kV. In addition, the monoclinic phase content was evaluated by calculating the phase composition according to the combined

formula of Garvie et al. [38] and Toraya et al. [39].

$$V_m = \frac{1.311 * [I_m(-111) + I_m(111)]}{1.311 * [I_m(-111) + I_m(111)] + I_t(101)}$$
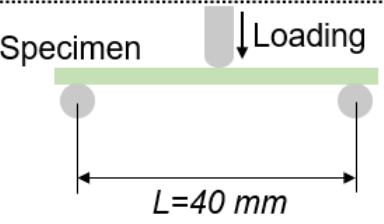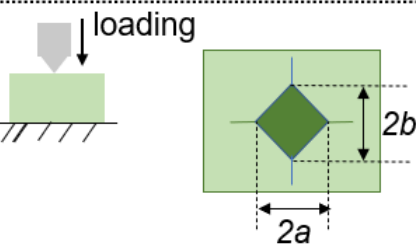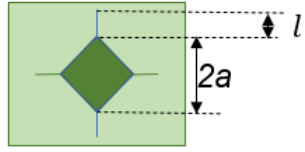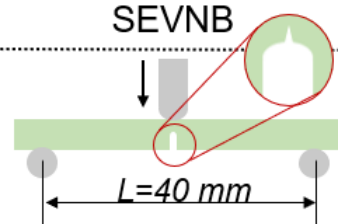
where V_m is the monoclinic phase volume fraction, $I_m(-111)$ and $I_m(111)$ are the monoclinic peak intensities corresponding to planes (-111) and (111), respectively, and $I_t(101)$ is the tetragonal peak intensity corresponding to the plane (101).

2.2.5 Mechanical properties

The mechanical properties, such as the Vickers hardness, three-point bending strength and fracture toughness were comprehensively investigated using the methods described in Table 2 at room temperature. Additionally, a Weibull analysis of the flexural strength data was conducted to describe the failure probability of zirconia. The fracture toughness value (K_{IC}) is evaluated by indentation and the single edge V-notched beam (SEVNB) method, respectively. Indentation methods are commonly used to evaluate the yields the crack initiation resistance, because the required specimens can be easily prepared and a large number of data can be obtained from one specimen [40]. However, it is unreliable due to subcritical crack growth and hence there is difficulty in determining the exact length of the cracks [41]. In addition, the selection of the equations depends on the crack type, so it is important to choose an appropriate equation based on the morphology of the actual indentation

cracking. In this study, the crack type was Palmqvist and the ratio of l (crack length) to a (half of diagonal length) was between 0.25-2.5; therefore, the equation introduced by Niihara et al. [42] was adopted for the calculation of K_{IC}. In contrast, an alternative method, the single edge V-notched beam (SEVNB) method, is considered as one of the most reliable methods, but the preparation of the V-notch is very challenging [43,44]. In this work, an ultra-sharp V-notch (ρ=0.5 μm, red dashed line in Fig. 5) was introduced by a femtosecond laser to obtain the accurate fracture toughness [45]. Fig. 5 shows that U-grooves with specific depths were cut by a low speed cutter with 200 μm thickness diamond wheels (IsoMet[TM], Buehler, LakeBluff, IL, USA) under water irrigation and then a sharp V-notch was induced at the bottom of U-grooves by the femtosecond laser (Pharos-10 W, Light Conversion, Lithuania) having a laser power of 2.9 W. The femtosecond lasers delivered 290 fs linearly polarised pluses at 515 nm with a repetition rate of 100 kHz. Finally, the SEVNB specimens were kept at 1200°C for 20 min to remove the machining stress.

Table 2. Mechanical property investigation methods.

	Flexural strength	Vickers hardness	Fracture toughness	
			Indentation	SEVNB
Schematic diagram				
Equation	$\sigma_f = 3PL/2bh^2$ P: Loading (N); L: Loading span (mm); b: samples width (mm); h: samples thickness (mm)	$HV = 0.0018544 \dfrac{P}{d^2}$ P: Loading (N); d: Average diagonal length of the indentation mark (mm)	$K_{IC} = 0.0089 \left(\dfrac{E}{H}\right)^{2/5} \dfrac{P}{al^{1/2}}$ E: Young's modulus (210 GPa); H: Hardness (GPa); P: Indentation load (N); a: half of diagonal length (m); l: crack length (m)	$K_{IC} = \dfrac{PL \times 10^{-6}}{BW^{3/2}} Y \dfrac{3\alpha^{1/2}}{2\beta^{3/2}}$ P: Loading (N); L: Loading span (mm); B: Samples thickness; W: Samples width; α: notch depth/sample width; $\beta = 1 - \alpha$; Y: dimensionless factor
Samples	N=40 Size: 45(L)*4(W)*3(H) mm	N=40 Size: 10(L)*10(W)*5(H) mm	N=40 Size: 10(L)*10(W)*5(H) mm	N=40 Size: 45(L)*4(W)*3(H) mm
Test standard	ASTM C1161-13	ASTM C1327-15	——	ASTM C1421-99
Test condition	0.5 mm/min, 1kN load cell	Loading: 98 N, dwell: 10s		0.5 mm/min, 1kN load cell
Instrument	Universal testing machine (LABSANS. Shenzhen, China)	Vickers hardness tester (THV-50MDX, Shanghai, China)		Universal testing machine
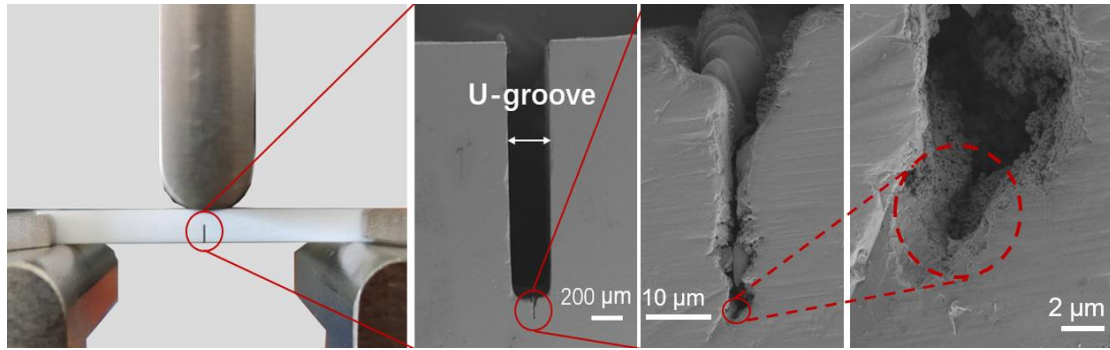
Fig. 5. Schematic diagram of SEVNB specimens.

3. Results and discussion

3.1 Densification studies

The degree of densification, which was evaluated in terms of both the relative density and by micro-CT, has considerable consequences for the mechanical properties of the 3D printed parts. The relative densities of the final parts were measured for 30 samples and an average value of 99.7 ± 0.2% of the theoretical density was obtained. A micro CT image of a sintered zirconia part is shown in Fig. 6, where the small number, location and size of defects is clearly seen – the latter are all believed to be pores arising from air entrapped within the slurry feedstock as the removal of the air bubbles in the viscous slurry is a significant challenge during the printing process. Overall, the microCT technique yielded a porosity value of only 0.00002%. It is believed that the pores could be reduced by decreasing the viscosity of slurry and/or by attaching a bubble removal device in the DLP printer.
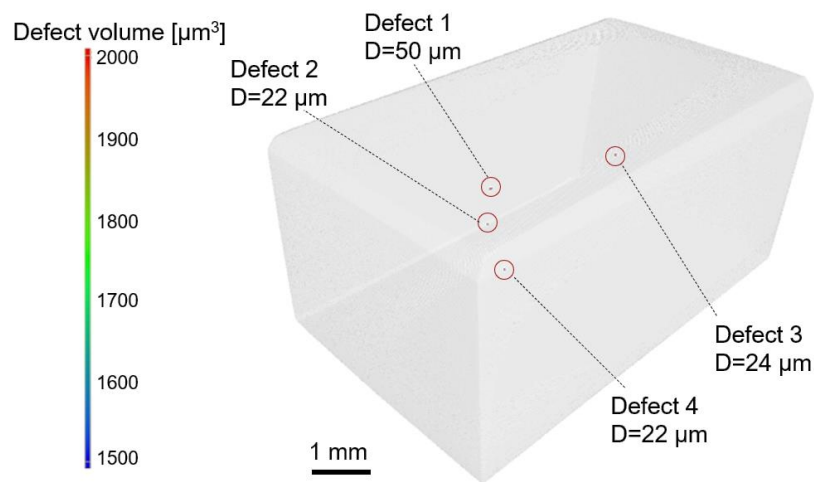
Fig. 6. Micro-CT 3D reconstructed image of zirconia part.

3.2 Sintering shrinkage, dimensional accuracy and surface roughness

As shown in Fig. 7a, crack- and distortion-free sintered zirconia bars were obtained. It is noted that uneven shrinkage during sintering is a common challenge that can directly affect the dimensional accuracy and sintering quality. It not only occurs with ceramics manufactured by AM processes, but also those made using traditional ceramic shaping processes [46]. In particular, an excessive sintering shrinkage can lead to shape deformation and the formation of micro-cracks [47]. In this study, Fig. 7b indicates that the sintering shrinkage was approximately equal in all three dimensions at ~23±0.15%, suggesting almost isotropic shrinkage. This isn't always, the case, however. For example, in 2019, we studied the sintering shrinkage of 3D printed zirconia parts and the measured values were 21.9% and 28.9% in the X-Y plane and Z direction, respectively. This difference was attributed to a low solid loading [5] and

different degrees of polymerisation occurring in the X-Y plane and Z direction

[48]; a low solids content slurry can also increase the risk of sample distortion

during sintering [49].
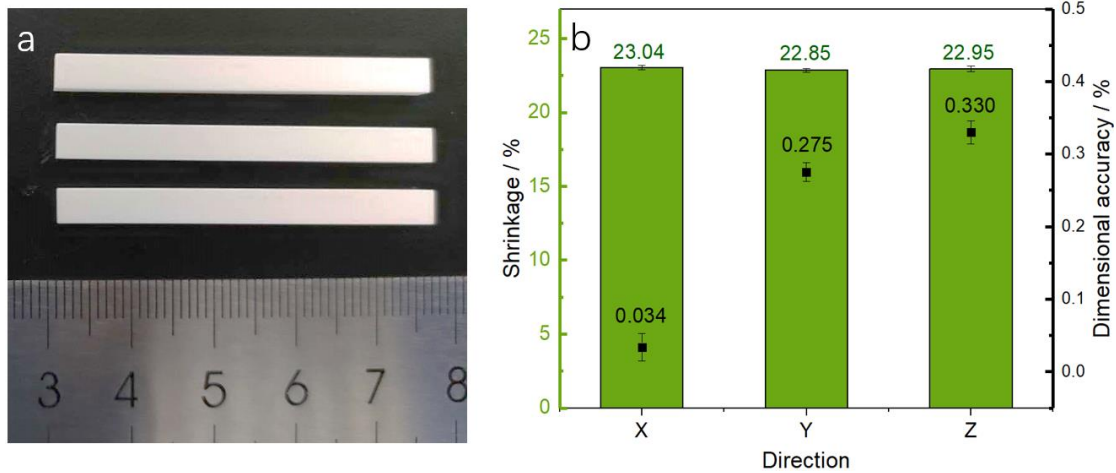
Fig. 7. (a) As-sintered zirconia bending bars and (b) the linear shrinkage and dimensional accuracy of the sintered parts.

Generally, a high-standard of dimensional accuracy is required to meet the

assembly requirements for high-end applications. As expected, AM-processed

parts yield different levels of dimensional tolerance as a result of post

processing steps, such as drying, debinding and sintering [50,51]. In this study,

the sintered dimensional accuracy was evaluated using 20 specimens with

defined dimensions of 45.0 × 4.0 × 3.0 mm. As shown in Fig 8, the average

dimensional tolerances obtained were less than ± 20 µm, which is similar to

what can be achieved using conventional subtractive manufacturing [49].
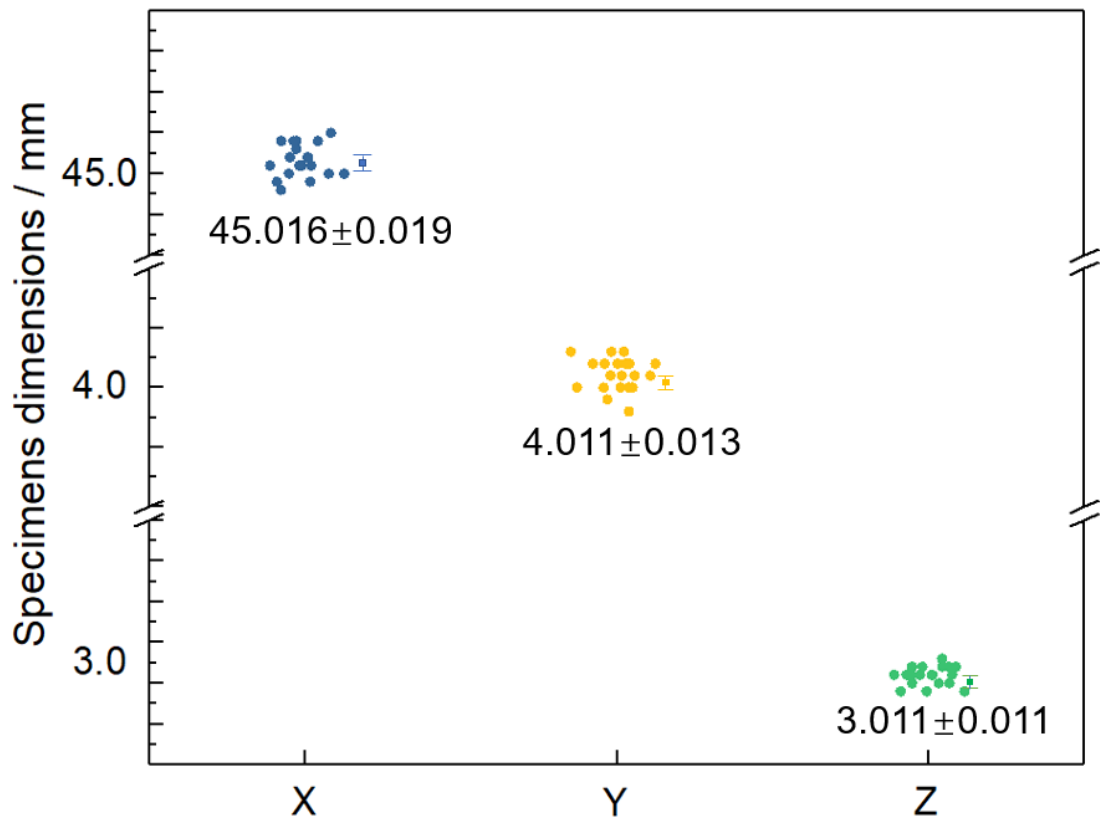
Fig 8. Measured dimensions of the sintered parts in X, Y and Z directions.

For many applications, e.g. in the aerospace and automobile industries, the surface roughness of parts is also important. Fig. 9 shows the values obtained in the present work and it will be observed that different levels of smoothness were obtained on the different surfaces. The top surface was the smoothest, with a mean Ra of just 1.62 μm; this is a measure of the smoothness of the deposition of the final layer. The bottom surface, however, was the roughest, with a mean Ra of 2.86 μm. The value is dependent on the surface quality of the build platform; in general, the latter is designed to have a rough texture to avoid the part detaching during the printing process. As can be seen, however, this leads to an undesirably high Ra. The sides of the part have intermediate

values of roughness; although they can be observed to have a step-like morphology, the resulting Ra value was only 2.19 μm.
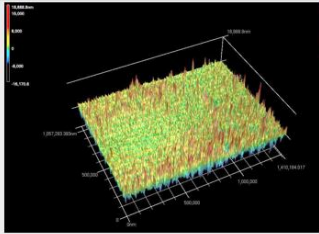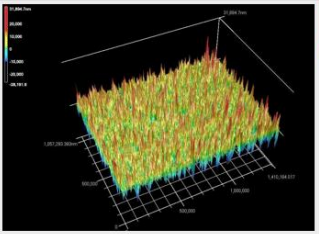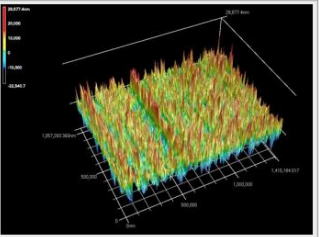
	Top surface	Side surface	Bottom surface
Ra (μm)	1.62 ± 0.23	2.19 ± 0.18	2.86 ± 0.12
Laser images			
3D images			

Fig. 9. Surface roughness and 3D topography of sintered parts.

3.3 Microstructural characterization

Fig. 10 (a) and (b) show the layered nature of the side surfaces, however no delamination or defects can be seen to occur between the layers. The smooth interlayer transition also supports the moderate surface roughness reported in section 3.2. Figure 10 (b) clearly shows that the thickness of each sintered layer was ~19 μm, which matches well with the 25 μm printing thickness given the sintering shrinkage in the Z direction. Fig. 10 (c) and (d) exhibit the microstructure of a thermally etched surface and its grain size distribution, respectively. The polished surface shows how dense the ceramic was and the grain boundaries can be easily observed; the average grain size was 259 ± 86

nm. As is known [52,53,54], the grain size has been demonstrated to be crucial for controlling the mechanical properties and low temperature degradation (LTD) of zirconia. Generally, as the grain size increases the strength of zirconia decreases due to a higher susceptibility to phase transformation, but, conversely, the fracture toughness increases [55]. In term of the LTD, a smaller grain size results in a decrease in the amount of t-m phase transformation, which can improve the resistance to LTD [56,57].
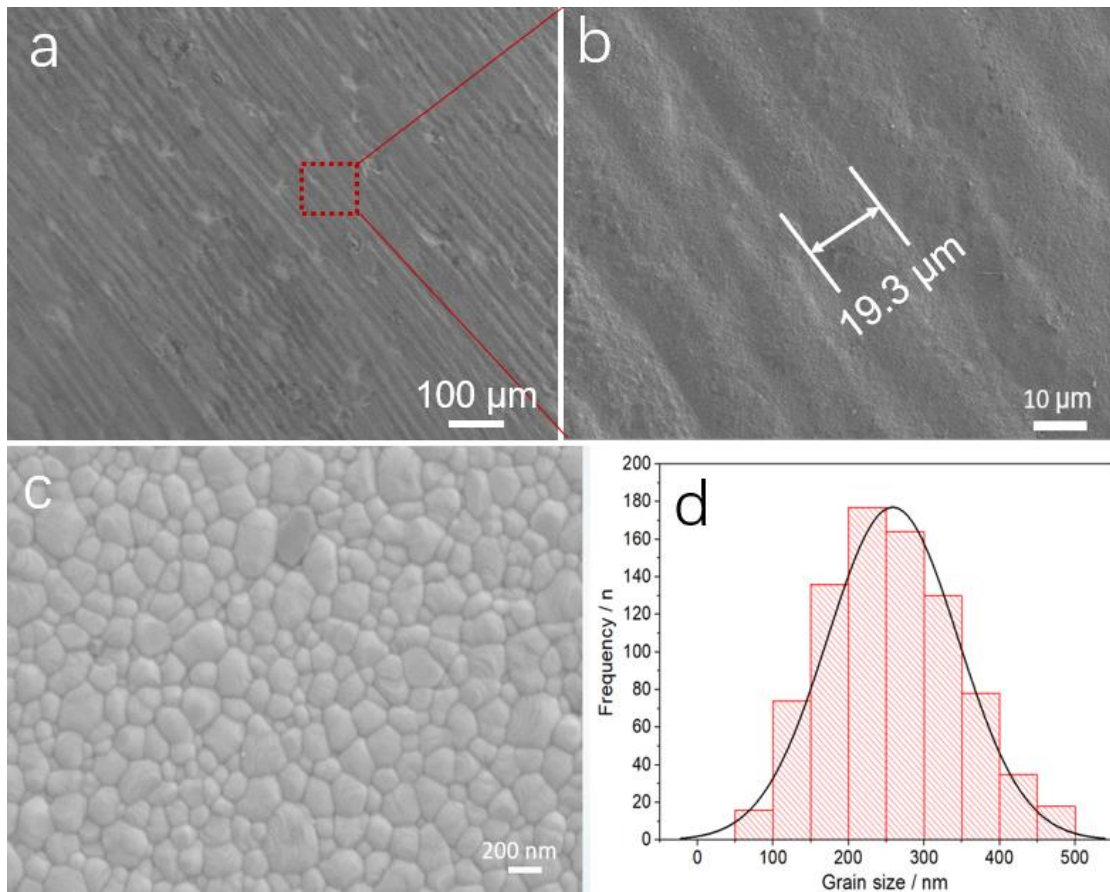
Fig. 10. SEM image of the: (a) layered structure at low magnification, (b) high magnification, (c) thermal etched surface, and (d) grain size distribution.

Fractographic analysis is one of the most reliable methods to identify the fracture mechanism. Fig. 11 shows fractographic images of an as-sintered specimen after fracture toughness testing. It was found that the origin of the failure started from the tip of the V-notch shown in the left image, as expected. SEM observation of the fractured surface revealed a mixture of intergranular and transgranular fracture. Generally, the high strength of the grain boundary leads to a transgranular fracture, which, ultimately, becomes intergranular. A zirconia sample exhibits an improved fracture toughness when failure occurs via the transgranular mode.
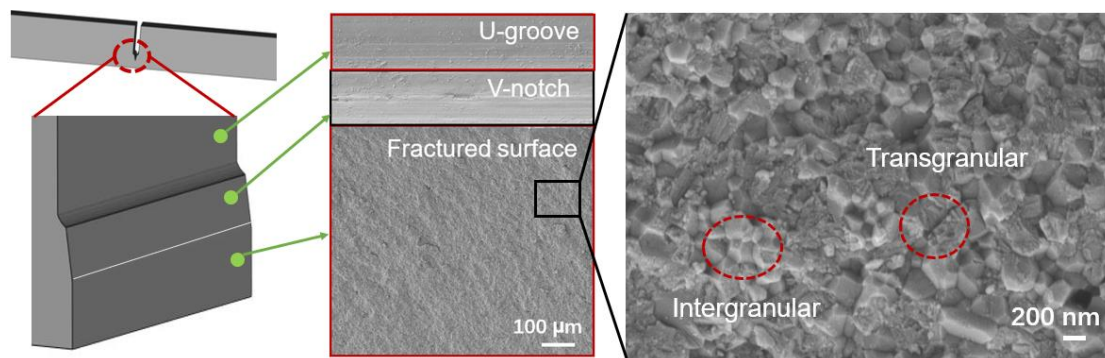
Fig. 11. Fracture surface of an SEVNB specimen showing the different regions (left images) and a high magnification micrograph of the resulting fractured surface (right image).

3.4 XRD analysis

Fig. 12 shows the crystalline phases present in the sintered zirconia before and after fracture. Whilst no significant monoclinic phase peaks were detected in the sintered samples before fracture, indicating that the 3Y-TZP was indeed stabilised in the tetragonal phase after sintering, monoclinic phase peaks were

observed at 2θ of 28.2°, 31.4° and 45.8° after fracture, demonstrating the occurrence of the t-m phase transformation during fracture. Quantitative analysis suggests that the volume percentage of the monoclinic phase after fracture was 18.9%, which is indicative of a promising fracture toughness [58][59].
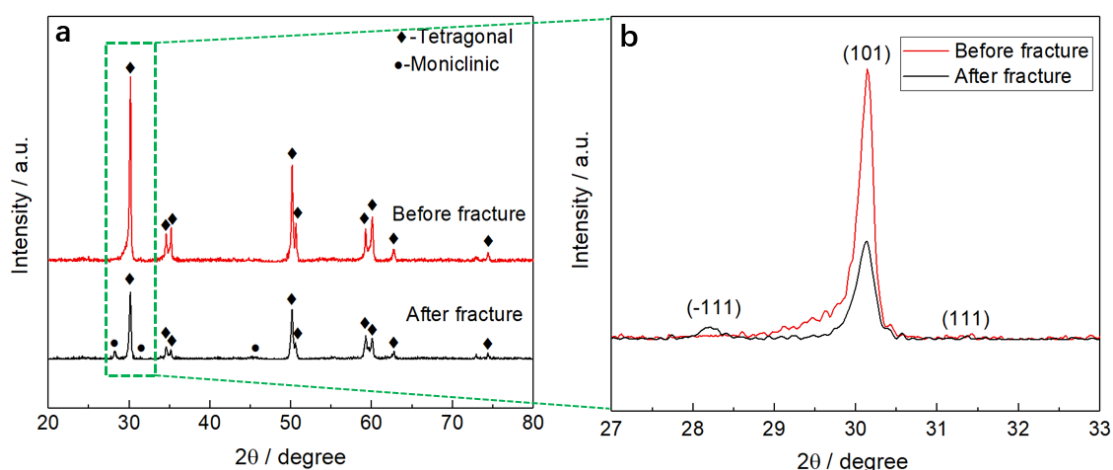
Fig. 12. XRD patterns of zirconia before and after fracture: (a) 2θ=20°–80°; (b) 2θ=27°–33°.

3.5 Mechanical properties

Table 3 presents the mechanical properties of the 3D printed zirconia. It is seen that the Vickers hardness and flexural strength values reached 12.59 ± 0.25 GPa and 1042 ± 75 MPa, respectively. Fig. 13 shows the Weibull plot for the 3-point flexural strength; a characteristic strength of 1076 MPa and Weibull modulus of 16.4 were obtained, which indicate the specimens were of high quality and reliability [60,61,62]. These favourable properties can be attributed to the high density and fine grain size of the parts manufactured in this study.

The fracture toughness (K_{IC}) was determined via two methods, viz. indentation and the SEVNB method. The results show that the K_{IC} obtained from the former method, 6.68 ± 0.17 MPa m$^{1/2}$, was higher than that obtained by the SEVNB method, 5.47 ± 0.28 MPa m$^{1/2}$. This is a common outcome and can be explained by the evaluation methods. Fischer et al. [62] have shown that the notch root radius of SEVNB specimens is extremely important for the evaluation of fracture toughness; the greater the radius, the higher the measured value of K_{IC}. In general, fracture toughness values obtained by the SEVNB method are in good agreement with the true value for zirconia when the notch-root radius is in the approximate range of 1.5 to 3 times the value of the mean grain size [62]. The latter was ~0.26 μm in this study whilst the notch-root radius was ~0.5 μm, see Fig. 5, suggesting that the fracture toughness value obtained by the SEVNB method was reliable and reproducible. In contrast, the indentation technique is known to be more of a measure of the crack initiation resistance than the fracture toughness [63][64].

Table 3. Mechanical properties of DLP manufactured zirconia

Hardness / GPa	3-point bending strength / MPa	Fracture toughness / MPa m$^{1/2}$	
		Indentation	SEVNB
12.59 ± 0.25	1042 ± 75	6.68 ± 0.17	5.47 ± 0.28
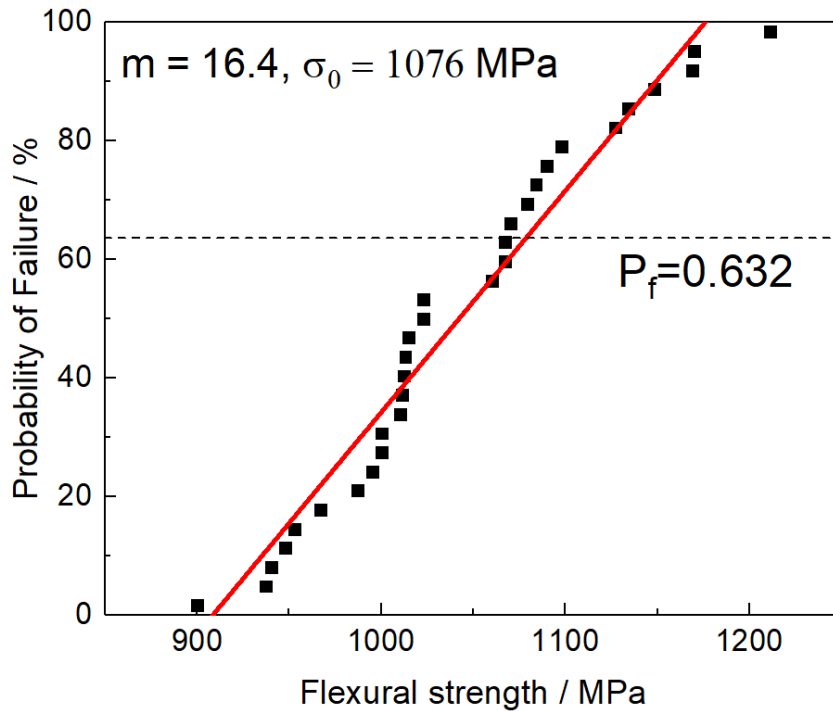
Fig. 13. Weibull plot of the flexural strength

The measured values of fracture toughness and flexural strength are compared to literature values for ceramics produced using 'conventional' routes in Fig. 14. It can be seen that the current DLP-printed zirconia exhibited comparable values, however, the DLP technique still presents challenges inherent to a technique based on the deposition of layers, including anisotropy in the mechanical properties, particularly flexural strength. Numerous efforts have been made to study the influence of the build direction on the mechanical properties. For example, Marsico et al. [65] indicated that the build orientation has a significant effect on the indentation fracture resistance and bend strength. Osman et al. [66] printed specimens in three different build angles (0°, 45° and 90°) for bending tests. The results revealed a significantly higher characteristic strength of 1006.6 MPa for the 0° fabricated specimens compared to the other

two groups, which had a mean of ~880 MPa. It is, therefore, a major task to minimize the anisotropic mechanical properties gap of components from the DLP process through optimizing the build direction.
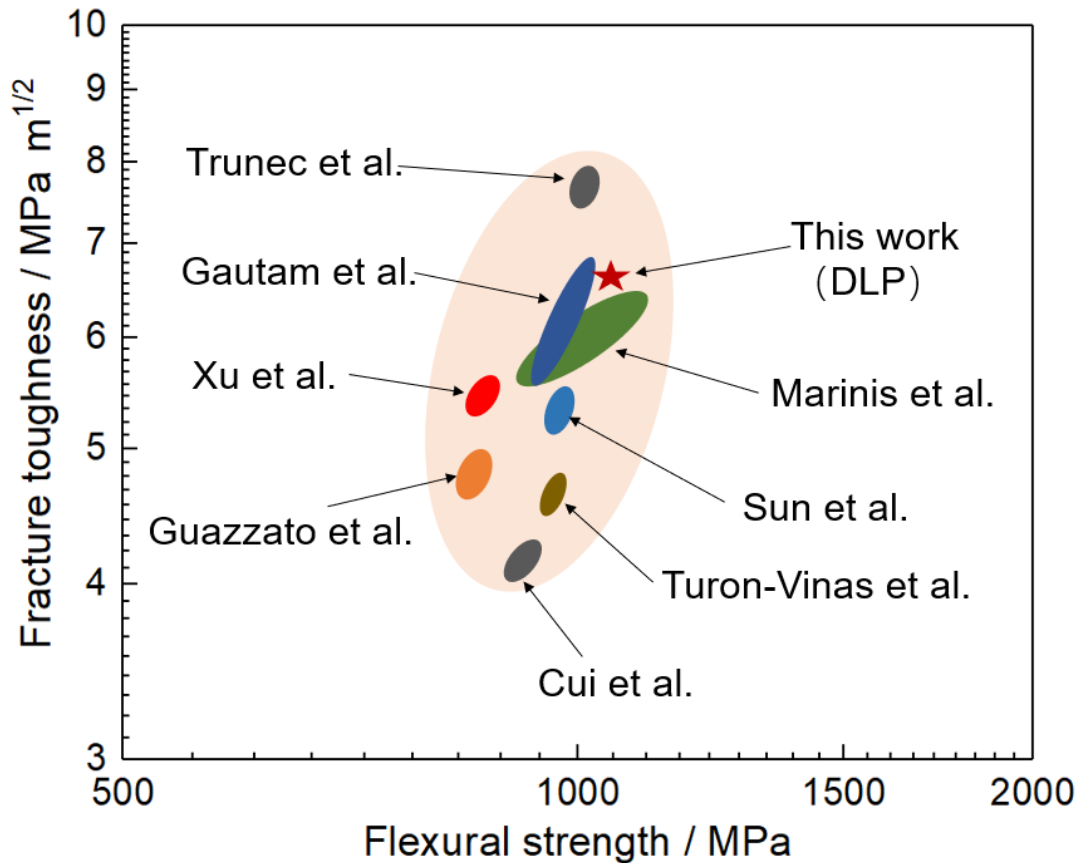
Fig. 14. Comparison of mechanical properties of zirconia made in this work and by conventional techniques [52,67,68,69,45,70,71].

3.6 Potential applications of processing zirconia by DLP

To demonstrate the tremendous potential of the DLP additive manufacturing technology to fabricate zirconia parts with functional complex geometries and sufficient surface finish, a range of zirconia parts were printed; they are shown in Fig. 15. These examples demonstrate that DLP-printed zirconia could be relevant for a range of industrial and biomedical applications, although further

work is still needed due to the anisotropic performance, slow build rates (at best, up to ~300 layers per hours at the lab scale; slower for commercial production) and small build volumes (less than 200 x 200 x 200 mm for most commercial DLP printers). However, the industrial community can be more confident about adopting AM to fabricate ceramic components that cannot be easily shaped by traditional methods.
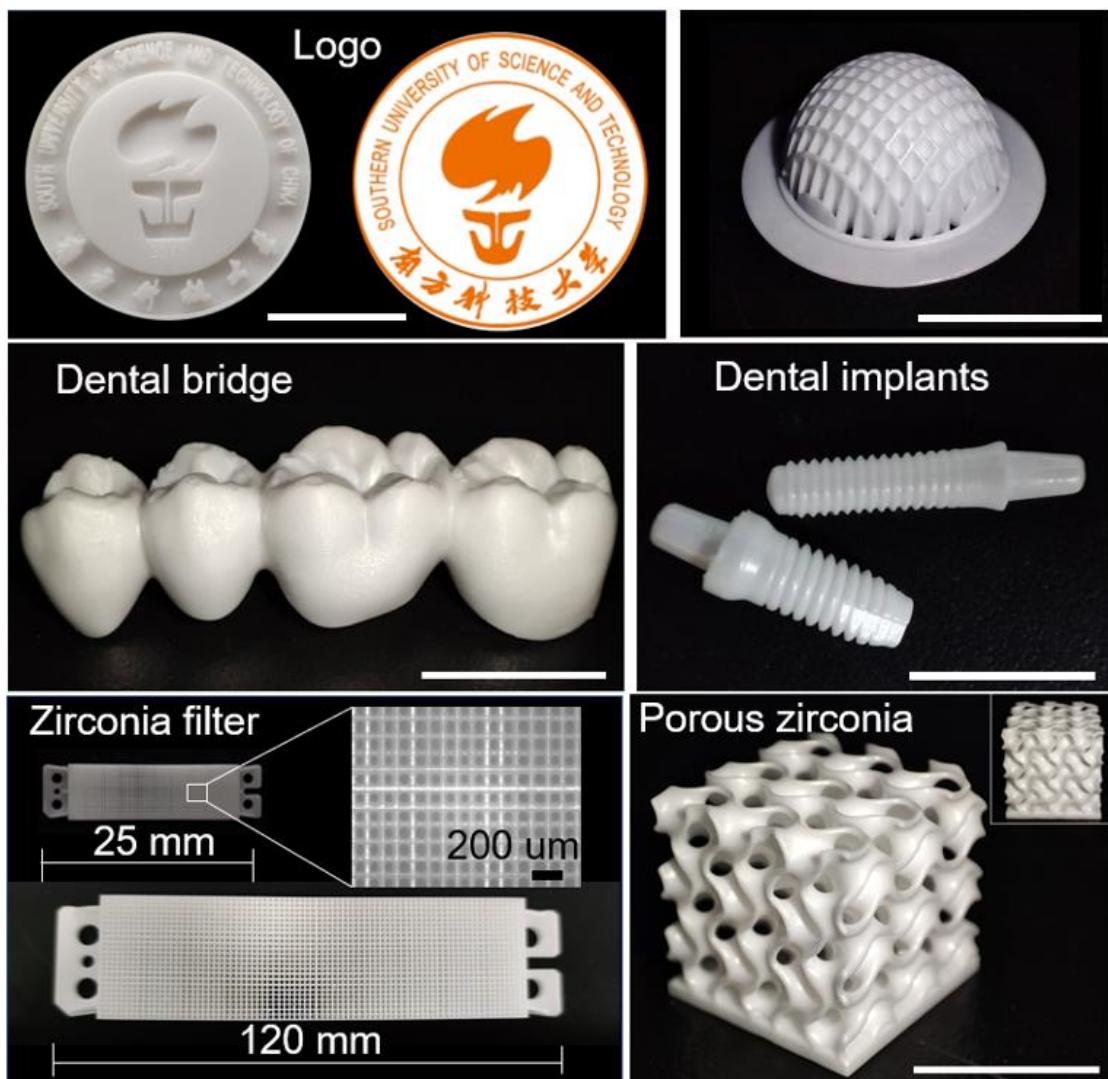
Fig. 15. DLP printed zirconia parts, scale bar: 10 mm in each image.

4. Conclusions

Digital light processing was employed to produce highly dense zirconia parts and their performance was comprehensively studied and compared to those of samples produced by traditional techniques. The results show that DLP is able to produce components with properties that are comparable to those of conventionally produced zirconia, although there is always a risk that the properties can be anisotropic with respect to the build direction.

More specifically, the results can be summarized as:

1. The relative density of the as-sintered zirconia was 99.7±0.2%, with the micro-CT images revealing only a small number of defects, which were believed to be porosity arising from air bubbles trapped in the slurry.

2. The sintering shrinkage was almost isotropic, being ~23±0.15%. This yielded dimensional errors of <0.33%, a value that would decrease with larger specimens.

3. The surface roughness varied across the difference sides of the samples; whilst the top surface was the smoothest, Ra = 1.62 μm, as expected, the sides had a slight step-like morphology and an Ra of 2.19 μm. Meanwhile, the bottom surface was the coarsest, with an Ra of 2.86 μm due to the need for the build plate to grip the samples as they were formed. Depending on the application, some machining of the bottom and sides may therefore be necessary.

4. No delamination was observed in the microstructure and the measured grain size was 259 ± 86 nm. Fractographic analysis revealed a mixed mode of intergranular and transgranular fracture.

5. A tetragonal to monoclinic phase transformation of 18.9% on the fracture surface is regarded as beneficial since it is indicative of a desirable level of fracture toughness.

6. The Vickers hardness and flexural strength were 12.59 ± 0.25 GPa and 1042 ± 75 MPa, respectively, which are comparable values to conventionally green formed and sintered zirconia. The difference in the fracture toughness values obtained by the SEVNB method, 5.47 ± 0.28 MPa m$^{1/2}$, and indentation technique, 6.68 ± 0.17 MPa m$^{1/2}$, is indicative of the different nature of the tests. A Weibull analysis showed that the printed specimens had high quality and high reliability.

7. Finally, samples with a range of shapes and sizes were fabricated to demonstrate the potential of the DLP technique.

Overall, it is felt that the technique is now ready to take the next steps towards industrialisation. The major issues still outstanding are the need for a final machining stage for many applications – particularly of the side and bottom surfaces (though this can also be true for conventionally-formed parts) and the slow build rates. The latter perhaps currently restrict the technique to the production of low volume products.

Declaration of competing interest

The authors declare that they have no known competing financial interests or personal relationships that could have influenced the work reported in this paper.

References

[1]　T. Chartier, C. Chaput, F. Doreau, and M. Loiseau, "Stereolithography of structural complex ceramic parts," *J. Mater. Sci.*, vol. 37, no. 15, pp. 3141–3147, 2002, doi: 10.1023/A:1016102210277.

[2]　T. Chartier *et al.*, "Additive manufacturing to produce complex 3D ceramic parts," *Journal of Ceramic Science and Technology*. 2015, doi: 10.4416/JCST2014-00040.

[3]　S. Zakeri, M. Vippola, and E. Levänen, "A comprehensive review of the

photopolymerization of ceramic resins used in stereolithography," *Addit. Manuf.*, vol. 35, no. March, p. 101177, 2020, doi: 10.1016/j.addma.2020.101177.

[4]   E. Zanchetta *et al.*, "Stereolithography of SiOC Ceramic Microcomponents," *Adv. Mater.*, vol. 28, no. 2, pp. 370–376, Jan. 2016, doi: 10.1002/adma.201503470.

[5]   J. Sun, J. Binner, and J. Bai, "Effect of surface treatment on the dispersion of nano zirconia particles in non-aqueous suspensions for stereolithography," *J. Eur. Ceram. Soc.*, Oct. 2018, doi: 10.1016/J.JEURCERAMSOC.2018.10.024.

[6]   W. Wang, J. Sun, B. Guo, X. Chen, K. P. Ananth, and J. Bai, "Fabrication of piezoelectric nano-ceramics via stereolithography of low viscous and non-aqueous suspensions," *J. Eur. Ceram. Soc.*, 2020, doi: 10.1016/j.jeurceramsoc.2019.10.033.

[7]   T. Zheng, W. Wang, J. Sun, J. Liu, and J. Bai, "Development and evaluation of Al2O3–ZrO2 composite processed by digital light 3D printing," *Ceram. Int.*, 2020, doi: 10.1016/j.ceramint.2019.12.102.

[8]   Y. H. Lee, J. Bin Lee, W. Y. Maeng, Y. H. Koh, and H. E. Kim, "Photocurable ceramic slurry using solid camphor as novel diluent for conventional digital light processing (DLP) process," *J. Eur. Ceram. Soc.*, 2019, doi: 10.1016/j.jeurceramsoc.2019.05.069.

[9]   E. Peng *et al.*, "Robocasting of dense yttria-stabilized zirconia structures," *J. Mater. Sci.*, 2018, doi: 10.1007/s10853-017-1491-x.

[10]   D. Zhang *et al.*, "A 3D-printing method of fabrication for metals, ceramics, and multi-materials using a universal self-curable technique for robocasting," *Mater. Horizons*, 2020, doi: 10.1039/c9mh01690b.

[11]   L. Rueschhoff, W. Costakis, M. Michie, J. Youngblood, and R. Trice, "Additive Manufacturing of Dense Ceramic Parts via Direct Ink Writing of Aqueous Alumina Suspensions," *Int. J. Appl. Ceram. Technol.*, 2016, doi: 10.1111/ijac.12557.

[12]   J. Liao, H. Chen, H. Luo, X. Wang, K. Zhou, and D. Zhang, "Direct ink writing of zirconia three-dimensional structures," *J. Mater. Chem. C*, 2017, doi: 10.1039/c7tc01545c.

[13]   S. J. Huang and C. S. Ye, "Preparation and performance of binder jetting porous alumina ceramic," *IOP Conf. Ser. Mater. Sci. Eng.*, 2020, doi: 10.1088/1757-899x/770/1/012057.

[14]   S. Huang, C. Ye, H. Zhao, Z. Fan, and Q. Wei, "Binder jetting yttria stabilised zirconia ceramic with inorganic colloid as a binder," *Adv. Appl. Ceram.*, 2019, doi: 10.1080/17436753.2019.1666593.

[15]   P. Kunchala and K. Kappagantula, "3D printing high density ceramics using binder jetting with nanoparticle densifiers," *Mater. Des.*, 2018, doi: 10.1016/j.matdes.2018.06.009.

[16]   X. Lv, F. Ye, L. Cheng, S. Fan, and Y. Liu, "Binder jetting of ceramics:

Powders, binders, printing parameters, equipment, and post-treatment,"

Ceramics International. 2019, doi: 10.1016/j.ceramint.2019.04.012.

[17]   J. Ebert *et al.*, "Direct inkjet printing of dental prostheses made of

zirconia," *J. Dent. Res.*, 2009, doi: 10.1177/0022034509339988.

[18]   B. Derby, "Additive Manufacture of Ceramics Components by Inkjet

Printing," *Engineering.* 2015, doi: 10.15302/J-ENG-2015014.

[19]   F. Chen, J.-M. Wu, H.-Q. Wu, Y. Chen, C.-H. Li, and Y.-S. Shi,

"Microstructure and mechanical properties of 3Y-TZP dental ceramics

fabricated by selective laser sintering combined with cold isostatic

pressing," *Int. J. Light. Mater. Manuf.*, 2018, doi:

10.1016/j.ijlmm.2018.09.002.

[20]   H. Yves-Christian, W. Jan, M. Wilhelm, W. Konrad, and P. Reinhart,

"Net shaped high performance oxide ceramic parts by Selective Laser

Melting," in *Physics Procedia*, 2010, doi: 10.1016/j.phpro.2010.08.086.

[21]   S. L. Sing *et al.*, "Direct selective laser sintering and melting of

ceramics: A review," *Rapid Prototyping Journal.* 2017, doi:

10.1108/RPJ-11-2015-0178.

[22]   S. Yan, D. Wu, F. Niu, Y. Huang, N. Liu, and G. Ma, "Effect of ultrasonic

power on forming quality of nano-sized Al2O3-ZrO2 eutectic ceramic via

laser engineered net shaping (LENS)," *Ceram. Int.*, 2018, doi:

10.1016/j.ceramint.2017.10.067.

[23] Z. Fan, Y. Zhao, M. Lu, and H. Huang, "Yttria stabilized zirconia (YSZ) thin wall structures fabricated using laser engineered net shaping (LENS)," *Int. J. Adv. Manuf. Technol.*, 2019, doi: 10.1007/s00170-019-03322-z.

[24] J. Raynaud *et al.,* "Hybridization of additive manufacturing processes to build ceramic/metal parts: Example of LTCC," *J. Eur. Ceram. Soc.*, vol. 40, no. 3, pp. 759–767, 2020, doi: 10.1016/j.jeurceramsoc.2019.10.019.

[25] A. Bravo-Leon, Y. Morikawa, M. Kawahara, and M. J. Mayo, "Fracture toughness of nanocrystalline tetragonal zirconia with low yttria content," *Acta Mater.*, 2002, doi: 10.1016/S1359-6454(02)00283-5.

[26] B. Basu, "Toughening of yttria-stabilised tetragonal zirconia ceramics," *Int. Mater. Rev.*, 2005, doi: 10.1179/174328005X41113.

[27] I. Denry and J. R. Kelly, "Emerging ceramic-based materials for dentistry," *Journal of Dental Research*. 2014, doi: 10.1177/0022034514553627.

[28] Z. Özkurt and E. Kazazoğlu, "Zirconia dental implants: A literature review," *Journal of Oral Implantology*. 2011, doi: 10.1563/AAID-JOI-D-09-00079.

[29] T. Chartier *et al.,* "Fabrication of millimeter wave components via ceramic stereo- and microstereolithography processes," *J. Am. Ceram.*

Soc., 2008, doi: 10.1111/j.1551-2916.2008.02482.x.

[30]   C. Marsico, M. Øilo, M. Kauf, and D. Arola, "Vat polymerization-printed

partially stabilized zirconia : Mechanical properties , reliability and

structural defects," vol. 36, no. June, 2020, doi:

10.1016/j.addma.2020.101450.

[31]   M. F. Ashby, "Materials selection in mechanical design," *Metall. Ital.*,

1994, doi: 10.1016/0956-7143(93)90102-e.

[32]   J. C. Wang, H. Dommati, and S. J. Hsieh, "Review of additive

manufacturing methods for high-performance ceramic materials,"

International Journal of Advanced Manufacturing Technology. 2019, doi:

10.1007/s00170-019-03669-3.

[33]   P. Colombo, G. Mera, R. Riedel, and G. D. Sorarù, "Polymer-derived

ceramics: 40 Years of research and innovation in advanced ceramics,"

J. Am. Ceram. Soc., 2010, doi: 10.1111/j.1551-2916.2010.03876.x.

[34]   R. Terao, J. Tatami, T. Meguro, and K. Komeya, "Fracture behavior of

AlN ceramics with rare earth oxides," *J. Eur. Ceram. Soc.*, 2002, doi:

10.1016/S0955-2219(01)00422-8.

[35]   E. Bernardo, P. Colombo, and E. Manias, "SiOC glass modified by

montmorillonite clay," *Ceram. Int.*, 2006, doi:

10.1016/j.ceramint.2005.05.002.

[36]   W. Wang, Z. Fu, H. Wang, and R. Yuan, "Influence of hot pressing

sintering temperature and time on microstructure and mechanical properties of TiB2 ceramics," *J. Eur. Ceram. Soc.*, 2002, doi: 10.1016/S0955-2219(01)00424-1.

[37] J. C. WURST and J. A. NELSON, "Lineal Intercept Technique for Measuring Grain Size in Two-Phase Polycrystalline Ceramics," *J. Am. Ceram. Soc.*, 1972, doi: 10.1111/j.1151-2916.1972.tb11224.x.

[38] R. C. GARVIE and P. S. NICHOLSON, "Phase Analysis in Zirconia Systems," *J. Am. Ceram. Soc.*, 1972, doi: 10.1111/j.1151-2916.1972.tb11290.x.

[39] H. Toraya, M. Yoshimura, and S. Somiya, "Calibration Curve for Quantitative Analysis of the Monoclinic-Tetragonal ZrO2 System by X-Ray Diffraction," *J. Am. Ceram. Soc.*, 1984, doi: 10.1111/j.1151-2916.1984.tb19715.x.

[40] D. Ćorić, M. Majić Renjo, and L. Ćurković, "Vickers indentation fracture toughness of Y-TZP dental ceramics," *Int. J. Refract. Met. Hard Mater.*, 2017, doi: 10.1016/j.ijrmhm.2016.12.016.

[41] K. Strecker, S. Ribeiro, and M. J. Hoffmann, "Fracture toughness measurements of LPS-SiC: A comparison of the indentation technique and the SEVNB method," in *Materials Research*, 2005, doi: 10.1590/S1516-14392005000200004.

[42] A. Şakar-Deliormanli and M. Güden, "Microhardness and fracture

toughness of dental materials by indentation method," *J. Biomed. Mater. Res. - Part B Appl. Biomater.*, 2006, doi: 10.1002/jbm.b.30371.

[43]   S. S. Scherrer, I. L. Denry, and H. W. A. Wiskott, "Comparison of three fracture toughness testing techniques using a dental glass and a dental ceramic," *Dent. Mater.*, 1998, doi: 10.1016/S0109-5641(98)00032-3.

[44]   J. Kübler, "Fracture Toughness of Ceramics Using the SEVNB Method: Round Robin," *VAMAS Rep.*, 1999, doi: 10.1520/STP10473S.

[45]   J. Cui, Z. Gong, M. Lv, and P. Rao, "Effect of notch depth on fracture toughness of zirconia ceramics tested by SEVNB method," *Ceram. Int.*, 2018, doi: 10.1016/j.ceramint.2018.06.179.

[46]   Z. Yang *et al.*, "Preparation of textured porous Al2O3 ceramics by slip casting in a strong magnetic field and its mechanical properties," *Cryst. Res. Technol.*, 2015, doi: 10.1002/crat.201500080.

[47]   H. Wu, D. Li, Y. Tang, B. Sun, and D. Xu, "Rapid fabrication of alumina-based ceramic cores for gas turbine blades by stereolithography and gelcasting," *J. Mater. Process. Technol.*, 2009, doi: 10.1016/j.jmatprotec.2009.07.002.

[48]   Q. Lian *et al.*, "Accurate printing of a zirconia molar crown bridge using three-part auxiliary supports and ceramic mask projection stereolithography," *Ceram. Int.*, 2019, doi: 10.1016/j.ceramint.2019.06.111.

[49] H. Li, L. Song, J. Sun, J. Ma, and Z. Shen, "Stereolithography-fabricated zirconia dental prostheses: concerns based on clinical requirements," *Adv. Appl. Ceram.*, 2020, doi: 10.1080/17436753.2019.1709687.

[50] X. Tian, D. Li, Z. Chen, and W. Zhou, "Study on the fabrication accuracy of ceramic parts by direct stereolithography," *Virtual Phys. Prototyp.*, 2012, doi: 10.1080/17452759.2012.718492.

[51] Z. Han *et al.*, "A Novel ZrO2 Ceramic Suspension for Ceramic Stereolithography," in *IOP Conference Series: Materials Science and Engineering*, 2019, doi: 10.1088/1757-899X/678/1/012021.

[52] M. Trunec, "Effect of grain size on mechanical properties of 3Y-TZP ceramics," *Ceram. - Silikaty*, 2008.

[53] S. Zang, N. He, X. Sun, M. Sun, W. Wu, and H. Yang, "Influence of additives on the purity of tetragonal phase and grain size of ceria-stabilized tetragonal zirconia polycrystals (Ce-TZP)," *Ceram. Int.*, 2019, doi: 10.1016/j.ceramint.2018.09.179.

[54] M. Inokoshi *et al.*, "Influence of sintering conditions on low-temperature degradation of dental zirconia," *Dent. Mater.*, 2014, doi: 10.1016/j.dental.2014.03.005.

[55] K. Nakamura, E. Adolfsson, P. Milleding, T. Kanno, and U. Örtengren, "Influence of grain size and veneer firing process on the flexural strength of zirconia ceramics," *Eur. J. Oral Sci.*, 2012, doi:

10.1111/j.1600-0722.2012.00958.x.

[56] T. J. Lucas, N. C. Lawson, G. M. Janowski, and J. O. Burgess, "Effect of grain size on the monoclinic transformation, hardness, roughness, and modulus of aged partially stabilized zirconia," *Dent. Mater.*, 2015, doi: 10.1016/j.dental.2015.09.014.

[57] S. Lawson, "Environmental degradation of zirconia ceramics," *Journal of the European Ceramic Society*. 1995, doi: 10.1016/0955-2219(95)00035-S.

[58] R. H. J. Hannink, P. M. Kelly, and B. C. Muddle, "Transformation toughening in zirconia-containing ceramics," *J. Am. Ceram. Soc.*, 2000, doi: 10.1111/j.1151-2916.2000.tb01221.x.

[59] J. A. Muñoz Tabares and M. J. Anglada, "Quantitative analysis of monoclinic phase in 3Y-TZP by raman spectroscopy," *J. Am. Ceram. Soc.*, 2010, doi: 10.1111/j.1551-2916.2010.03635.x.

[60] M. Borlaf, A. Serra-Capdevila, C. Colominas, and T. Graule, "Development of UV-curable ZrO2 slurries for additive manufacturing (LCM-DLP) technology," *J. Eur. Ceram. Soc.*, 2019, doi: 10.1016/j.jeurceramsoc.2019.05.023.

[61] W. Harrer, M. Schwentenwein, T. Lube, and R. Danzer, "Fractography of zirconia-specimens made using additive manufacturing (LCM) technology," *J. Eur. Ceram. Soc.*, 2017, doi:

10.1016/j.jeurceramsoc.2017.03.018.

[62] H. Fischer, A. Waindich, and R. Telle, "Influence of preparation of ceramic SEVNB specimens on fracture toughness testing results," *Dent. Mater.*, 2008, doi: 10.1016/j.dental.2007.06.021.

[63] B. R. LAWN and D. B. MARSHALL, "Hardness, Toughness, and Brittleness: An Indentation Analysis," *J. Am. Ceram. Soc.*, 1979, doi: 10.1111/j.1151-2916.1979.tb19075.x.

[64] T. To, L. R. Jensen, and M. M. Smedskjaer, "On the relation between fracture toughness and crack resistance in oxide glasses," *J. Non. Cryst. Solids*, 2020, doi: 10.1016/j.jnoncrysol.2020.119946.

[65] C. Marsico, M. Øilo, J. Kutsch, M. Kauf, and D. Arola, "Vat polymerization-printed partially stabilized zirconia: Mechanical properties, reliability and structural defects," *Addit. Manuf.*, vol. 36, no. July, 2020, doi: 10.1016/j.addma.2020.101450.

[66] R. B. Osman, A. J. van der Veen, D. Huiberts, D. Wismeijer, and N. Alharbi, "3D-printing zirconia implants; a dream or a reality? An in-vitro study evaluating the dimensional accuracy, surface topography and mechanical properties of printed zirconia implant and discs," *J. Mech. Behav. Biomed. Mater.*, 2017, doi: 10.1016/j.jmbbm.2017.08.018.

[67] Y. hai Sun, Y. feng Zhang, and J. kun Guo, "Microstructure and bending strength of 3Y-TZP ceramics by liquid-phase sintering with CAS

addition," *Ceram. Int.*, 2003, doi: 10.1016/S0272-8842(02)00097-4.

[68] C. Gautam, J. Joyner, A. Gautam, J. Rao, and R. Vajtai, "Zirconia based dental ceramics: structure, mechanical properties, biocompatibility and applications," *Dalt. Trans.*, 2016, doi: 10.1039/c6dt03484e.

[69] A. Marinis *et al.*, "Fracture toughness of yttria-stabilized zirconia sintered in conventional and microwave ovens," *J. Prosthet. Dent.*, 2013, doi: 10.1016/S0022-3913(13)60037-2.

[70] M. Turon-Vinas and M. Anglada, "Strength and fracture toughness of zirconia dental ceramics," *Dental Materials*. 2018, doi: 10.1016/j.dental.2017.12.007.

[71] M. Guazzato, M. Albakry, S. P. Ringer, M. V. Swain, "Strength, fracture toughness and microstructure of a selection of all-ceramic materials . Part II. Zirconia-based dental ceramics," *Dental materials*. 2004, doi: 10.1016/j.dental.2003.05.002.